Dynamic utilization of low-molecular-weight organic substrates across a microbial growth rate gradient

K. Taylor Cyle[1], Annaleise R. Klein[2,4], Ludmilla Aristilde[2,3], Carmen Enid Martínez[1#]

[1]Soil and Crop Sciences, School of Integrative Plant Science, College of Agriculture and Life Sciences, Cornell University, Ithaca, NY, 14853, USA

[2]Department of Biological and Environmental Engineering, Cornell University, Riley-Robb Hall, Ithaca, NY 14853

[3]Department of Civil and Environmental Engineering, McCormick School of Engineering and Applied Science, Northwestern University, Evanston, IL, 60208, USA

[4]Australian Synchrotron, Australian Nuclear Science and Technology Organisation, Clayton, VIC 3168 Australia.

Corresponding Author

#email: cem20@cornell.edu

Keywords

Ecophysiology, nominal oxidation state of carbon, low molecular weight, time-resolved metabolic footprinting, carbon use efficiency

Abstract

Constantly in flux, low-molecular-weight organic substances (LMWOSs) are at the nexus between microorganisms, plant roots, detritus, and the soil mineral matrix. Nominal oxidation state of carbon (NOSC) has been put forward as one way to parameterize microbial uptake rates of LMWOSs and efficiency of carbon incorporation into new biomass. In this study, we employed an ecophysiological approach to test these proposed relationships using targeted exometabolomics (^{1}H-NMR, HR-LCMS) coupled with stable isotope (^{13}C) probing. We assessed the role of compound class and oxidation state on uptake kinetics and substrate-specific carbon use efficiency (SUE) during the growth of three model soil microorganisms (*Penicillium spinulosum*, *Paraburkholderia solitsugae,* and *Ralstonia pickettii*) in media containing 34 common LMWOSs. Microbial isolates were chosen to span a gradient in growth rate (0.046-0.316 hr^{-1}) and differ phylogenetically (a fungal isolate and two bacterial isolates). Clustered, co-utilization of LMWOSs occured for all three organisms, but temporal cluster separation was most apparent for *P. solitsugae*. Potential trends ($p < 0.05$) for early utilization of more oxidized substrates were present for the two bacterial isolates (*P. solitsugae* and *R. pickettii*), but high variability ($R^2 > 0.15$) and a small effect of NOSC indicate these are not useful relationships for prediction. The SUEs ranged from 0.16-0.99 and the hypothesized inverse relationship between NOSC and SUE was not observed. Thus, our results do not provide compelling support for NOSC as a predictive tool, implying that metabolic strategies of organisms may be more important than chemical identity in determining LMWOS cycling in soils.

Importance

Community-level observations from soils indicate that low-molecular-weight compounds of higher oxidation state tend to be depleted from soil solution faster and incorporated less efficiently into microbial biomass under oxic conditions. Here, we tested hypothetical relationships between substrate chemical characteristics and the order of substrate utilization by aerobic heterotrophs at the population-level in culture, using two bacterial isolates (*Ralstonia pickettii* and *Paraburkholderia solitsugae*) and one fungal isolate from soil (*Penicillium spinulosum*). We found weak relationships indicating earlier uptake of more oxidized substrates by the two bacterial isolates but no relationship for the fungal isolate. We found no relationship between substrate identity and substrate use efficiency. Our findings indicate that substrate chemical characteristics have limited utility for modeling the depletion of low-molecular-weight organics from soil solution and incorporation into biomass over broader phylogenetic gradients.

Introduction

Low-molecular-weight organic substances (LMWOSs) represent the interface between the microbial cell and the decomposition of organic inputs into soil and have long been understood to be critical to soil processes (1, 2). This pool of soil organic carbon is a relatively small fraction of total dissolved organic carbon at any one point in time, with concentrations of individual compounds typically at less than 1 mM (3). Rapid cycling of LMWOSs involves their partitioning into microbial biomass, metabolic respiration to CO_2, and contribution to the formation of mineral-associated organic matter (MAOM) (4, 5). The LMWOSs are released into solution through the action of exoenzymes depolymerizing particulate plant material and actively exuded by plant roots to shape soil microbial communities (6), thus altering soil solution nutrient

composition (7). While there is an emerging understanding of the complex signaling roles of LMWOSs (8), they primarily serve as the currency of the subterranean economy, providing both the carbon and energy source to support heterotrophic microbial populations. Therefore, a mechanistic understanding of microbial uptake and transformation of LMWOSs is warranted as this is the process through which the majority of soil respiration is produced (9) and a pivotal step in the formation of MAOM (10).

In fact, microbial uptake of LMWOSs in soil solution is much faster than sorption onto soil particles, thus highlighting the importance of microbial processing on the long-term fate of LMWOS-derived carbon and nitrogen in soils (11). Uptake rates tend to be extremely rapid (< 30 min) and previous studies have indicated that the half-life of the compound in soil is influenced by the compound class (3, 12). More oxidized compounds, such as organic acids, have been shown to be removed from soil solution and appear in respired CO_2 at faster rates than less oxidized compounds, such as sugars and amino acids (4, 13-16). Isotope (^{13}C, ^{14}C) tracer experiments have shown different affinity of cellular transport systems involved in uptake (17) by thousands of taxa (18).

Once transported within a microbial cell, LMWOSs are routed through metabolic pathways and incorporated into biomass production (anabolism, assimilation) or mineralized to CO_2 while producing reducing equivalents (catabolism, dissimilation) (19, 20). Accurately modeling the partitioning between anabolism and catabolism, referred to as carbon use efficiency (CUE), is critical to forecasting future changes in the soil carbon sink (21-23). Carbon use efficiency has been observed to vary due to intrinsic physiological strategies (e.g., growth rate, genome size) as well as to external conditions (e.g., temperature, moisture, substrate quality, nutrient limitations) (24-26). At the scale of individual compounds, the internal energy content of

the substrate being metabolized (denoted here as nominal oxidation state of carbon, NOSC) is one promising determinant of CUE (19, 27, 28). In this framework, due to energy limitations, the metabolism of the relatively more oxidized LMWOSs (higher NOSC) (e.g., organic acids) is hypothesized to result in lower assimilation efficiencies when these substrates are used as sole carbon sources. While the prevalence of oxygen in surface soils is typically considered to relieve thermodynamic limitations, recent field and laboratory observations have shown thermodynamics to still be a key regulator of aerobic respiration in carbon-limited aquatic systems (29-31) and this is supported by observations in intact soils as well (15).

Moreover, it is not likely that substrates are used sequentially by microbial populations when inhabiting environments containing diverse, low-concentration LMWOSs (32-34). Microbial metabolism may leverage the ability to route LMWOS-carbon from individual substrates divergently to anabolism or catabolism, thus producing specific substrate use efficiencies (SUE) that differ from relationships predicted from growth on a single substrate alone (19). Metabolomics using isotope labeling have observed nonuniform metabolic routing of assimilated substrates (35) and demonstrated the dynamic activation of specific metabolic pathways coinciding with the clustered, co-utilization of substrates in model organisms (36).

There is accumulated evidence that molecular size, compound class, and NOSC may be useful predictors uptake kinetics and use efficiency of LMWOS in soils and these concepts are being incorporated into substrate explicit modeling frameworks (37, 38). It is currently unclear whether correlations between compound characteristics and substrate utilization patterns (39) can be broadly applied to all aerobic heterotrophs in soil environments or whether these correlations simply arise from niche partitioning (e.g., faster-growing community members prefer to metabolize more oxidized substrates than slower-growing community members) (39). Therefore,

there is a need to conduct ecophysiological studies to understand substrate utilization profiles and metabolic use across the breadth of microbial diversity in soil. Though reductionist by design, studies of this category are necessary for asking fundamental questions about the influence of substrate chemistry on the microbial metabolism of carbon and for providing parameter bounds to modelers. They may show utility for building predictive models of microbial community interactions (40) and complementing observations from the field when done under realistic conditions of substrate diversity and concentration (41).

Here the aim of our study was to investigate the role of compound class and NOSC on substrate utilization profiles, uptake rates, and use efficiency at the microbial population level. For this work, we have grown three microbial strains isolated from a forest soil in a defined media with 34 LMWOSs at realistic, equimolar concentrations (25 μM each). The chosen isolates represented distinct phylogenies, an ascomycete (*Penicillium spinulosum*) and two closely related to Betaproteobacteria (*Paraburkholderia solitsugae, and Ralstonia pickettii*), which exhibited a range of growth rates in the defined media. We put forth three hypotheses: (1) that there is a negative relationship between substrate NOSC and the midpoint of substrate uptake; (2) that there is a negative relationship between NOSC and SUE; (3) that individual SUEs would diverge widely from the cumulative CUE in accordance with co-utilization and segregated routing of carbon substrates within carbon metabolism. We employed time-resolved exometabolomics to characterize the depletion of compounds from extracellular solution during their growth. Here, substrate depletion in the extracellular media is assumed to be due to cellular uptake. Parallel experiments using treatments with selective isotopically labeled LMWOS were performed to determine SUE in a mixed-substrate media. Our findings provide insights on the

utility of the inherent chemical characteristics of potential substrates as predictors of microbial preferences and usage efficiencies.

Results

Faster growth led to increased biomass production. The chosen microbial isolates, which ranged in growth rate in minimal defined media, exhibited a normalized specific growth rate (μ) of 0.04-0.32 hr^{-1} (Table 1, Fig. S1). The bacterial isolates (*R. pickettii*, *P. solitsugae*) grew faster and exhibited much shorter lag times than the fungal isolate (*P. spinulosum*) (Table 1, Fig. S1). Despite having a longer lag phase than *P. solitsugae*, the fastest growing isolate, *R. pickettii*, produced the most biomass in the shortest time (Table 1). Accordingly, the biomass data collected from labeled growth trials show that *R. pickettii* produced more cellular biomass (in mg) per OD unit (higher *k*) than *P. solitsugae*. While *R. pickettii* and *P. spinulosum* had similar cellular carbon contents, *P. solitsugae* had substantially less carbon per cellular dry mass (Table 1). These results showed the choice of isolates represented a gradient in growth rates, with faster growth resulting in more biomass but not necessarily more biomass carbon.

Clustered LMWOS utilization in terms of compound class and NOSC. Throughout their growth, the three microbial isolates depleted nearly all LMWOS by at least 50% from the initial concentrations in the extracellular media (Fig. 1, Fig. S3-S5). The transposition of modeled substrate uptake inflection points of (t_{50}) and usage time windows onto the growth curve of the isolate allowed comparisons of substrate usage patterns and usage overlap (Fig. 1). Using a k-means approach, three distinct uptake clusters (Cluster A, B, C) were identified for each isolate (Fig. 1A, 1C, 1E). The uptake of LMWOS occurred continuously whereby t_{50} values for substrates were distributed throughout the growth curve (Fig. 1B, 1D, 1F). Between the

isolates, the clearest temporal separation of clusters was evident during substrate uptake by *P. solitsugae* (Fig. 1C), partially due to the presence of t_{50} values early during the growth curve which were assigned to Cluster A (Fig. 1D). During the growth of *P. solitsugae*, a large proportion of each Cluster A substrate was depleted from the media (~75%, 12 h) before significant depletion of any Cluster B and C substrates (Fig. 1D). Clustering of substrate uptake for *R. pickettii* (Fig. 1A) and *P. spinulosum* (Fig. 1E) produced uptake groups with less temporal distinction and t_{50} values more closely centered around the midpoint of total carbon depletion than observed for *P. solitsugae* (Fig. 1D-E, Fig. S2). Greater than 70% of organic acid substrates were present in the earliest cluster for both bacterial isolates (Fig. 1B, 1D, Fig. 2A-B). Few compounds had significant early uptake by the fungus, *P. spinulosum,* with cluster A comprised of cysteine, gluconate, and the much slower uptake of glycine (Fig. 1F). In contrast to the bacterial isolates, *P. spinulosum* assimilated all organic acids except for gluconate in the last cluster, Cluster C (Fig. 1F, Fig. 2C). Clusters A and B were depleted completely for both bacterial isolates (Fig. 1A, 1C), while only Cluster B was depleted completely for *P. spinulosum* (Fig. 1E).

We did not obtain compelling evidence of a correlation between substrate NOSC and substrate t_{50} for any isolate (Fig. 2). The strongest potential trends were observed for *R. pickettii* and *P. solitsugae,* where the overall linear relationship between NOSC and the mean midpoint of substrate depletion (normalized t_{50}) could be explained by the equations (normalized t_{50} = 0.664 – 0.045 NOSC, adj R^2 = 0.101, p = 0.05) and (normalized t_{50} = 0.572 – 0.127 NOSC, adj R^2 = 0.146, p = 0.019), respectively (Fig. 2A-B), These potential trends appear to be driven by the earlier average uptake of organic acids as compared to amino acids by both isolates (t-test results are p = 0.037, p < 0.001, respectively) (Fig. 2B-C). No significant correlation was observed for

LMWOS uptake for *P. spinulosum* (Fig. 2C, p = 0.974), mostly due to the later uptake of three organic acids (malate, fumarate, α-ketoglutarate), though there was a trend for the earlier uptake of more oxidized amino acids (normalized t_{50} = 0.489 – 0.040 NOSC, adj R^2 = 0.232, p = 0.014). Despite a significant p-value (< 0.05) for some linear regression models in relation to the hypothesis of a correlation between NOSC and substrate utilization, all the linear regression models had a low adjusted R^2 (< 0.25), which indicated high variability, and a small slope (< 0.13 NOSC), which indicated a relatively minor effect of NOSC unit on the midpoint of substrate depletion (regressions not shown).

Maximum substrate depletion rates decayed exponentially during population growth when displayed as a biomass normalized rate (Fig. 3A-C, Table S2-S4). Biomass-normalized substrate depletion rates were generally below 6.10 μmol h^{-1} mg_{CDW}^{-1} for the two bacterial isolates (Fig. 3D-E, Table S2-S3), but the fungal biomass-normalized substrate depletion rates were much lower, predominantly below 0.15 μmol h^{-1} mg_{CDW}^{-1} (Fig. 3F, Table S4). Though organic acids generally trended towards higher biomass-normalized depletion rates for the *P. solitsugae* (Fig. 3), no significant differences between depletion rates by compound classes were observed for any isolate.

Substrate respiration dynamics, growth efficiency and substrate use efficiency of selected substrates. Labeled growth trials were used to track 5 specific substrates (glucose, acetate, formate, glycine, valine) that ranged in NOSC (-0.8 – 2) in the defined media (Fig. 4). All labeled substrates were respired (e.g., converted to CO_2) to various degrees (Fig. 4A-C). The production of respired $^{13}CO_2$ could be modeled in all cases except for *R. pickettii*'s respiration of ^{13}C-formate (Fig. 4A, Table S5). Though insufficient data from early portions of the growth curve prevented fitting, the t_{50} of ^{13}C-formate respiration must have been less than 11.5 hours

which was the first sampling time (Fig. 4A). In terms of initial media concentrations, the cumulative substrate-derived carbon that was respired from labeled substrates (CO_2-C, *a*) straddled the proportion for all carbon sources for all isolates (Fig. 4A-C, Table S5). Cumulative respired CO_2-C ranged from 12.74-25.29% of LMWOS-carbon present in the media (Fig. 4A-C, Table 5S). In all cases, carbon from the organic acids and sugar (acetate, formate, and glucose) appeared in respired CO_2 earlier (lower t_{50}) and more rapidly (smaller *w*) than the average of all carbon substrates (Fig. 4A-C, Table S5). The t_{50} of respiration of these three substrates ranged from 0.19-6.07 h before the average of all substrates for bacterial isolates and 13.5-19.52 h for the fungal isolate (Fig. 4A-C, Table S5). The cumulative proportion of formate-carbon in respiration was at least 1.77-fold higher than any other substrate for all isolates and ranged from 19.84-59.19% of added substrate-carbon (Fig. 4A-C, Table S5). The two amino acids, glycine and valine, had respiratory curves that were later (higher t_{50}) than overall CO_2 production for all isolates (Fig. 4A-C, Table S5). This was most pronounced for valine for the two bacterial isolates, where valine was not respired until the beginning of stationary phase, representing a delay of greater than 3.09 h from the average of all LMWOSs respired, or greater than 16.3% of the total growth curve (Fig. 4A-B, Table S5). In contrast, respiration of glycine and valine much more closely followed overall respiration for *P. spinulosum*, with differences in t_{50} ranging from 0.5-4.05 h or less than 4.2% of the total growth curve (Fig. 4C).

Estimates of SUE produced values ranging from 0.16-0.99 (Fig. 4D-I, Fig. S7). The largest divergence in SUEs between highest and lowest efficiencies was found during the growth of *P. solitsugae* (Fig. 4E, 4H). For the two bacterial isolates, *R. pickettii* and *P. solitsugae*, substrates that appeared in respired CO_2 earlier (lower t_{50}) than the other substrates had relatively lower SUEs (SUE = 0.027 t_{50} + 0.418, p = 0.025 and SUE = 0.078 t_{50} - 0.807, p = 0.011,

229 respectively) (Fig. 4D-E). There was no obvious trend between substrate respiration kinetics and
230 SUE for *P. spinulosum* (Fig. 4F). Both *R. pickettii* and *P. spinulosum* exhibited a smaller range
231 of SUE values, all of which (except formate) were at or near the overall CUE value, which was
232 0.84 and 0.76, respectively (Fig. 4G, 4I). These two isolates had a higher CUE than *P.*
233 *solitsugae,* whose CUE was estimated at 0.54 (Fig. 4H). Formate had a significantly lower SUE
234 for all isolates, never exceeding 0.31. No significant trends ($p < 0.1$) between the NOSC and
235 SUE were found for any isolate (Fig. 4G-I).
236
237 **Discussion**
238 This study aimed to characterize the substrate utilization profiles, uptake rates, and
239 metabolic partitioning of carbon (CUE, SUE) of three soil microbial isolates with different
240 growth rates. Using equimolar LMWOS concentrations and a diversity of substrates reflecting
241 those present at the field site of isolation (32), we aimed to investigate the role of substrate
242 energy content (NOSC) without confounding concentration differences. Stationary phase was
243 chosen as the point of assessment for population-level carbon use efficiency (CUE_p) to minimize
244 the influence of secondary metabolite turnover on respiration measurements (21). While
245 LMWOS are re-supplied in soil solution frequently, especially in the rhizosphere, these
246 experiments mimic resource pulse events that induce microbial growth.
247 **Faster growth did not result in lower CUE.** Specific bacterial phyla, such as
248 Betaproteobacteria and Bacteroidetes, are known to grow rapidly in response to resource-pulses
249 and this rapid growth is correlated positively to C-amendment levels in soil (42). Though the
250 fungal community often represents a larger proportion of total microbial biomass (43),
251 fungal:bacterial ratios derived from growth-based measurements made in C-units show bacterial

252 dominance (F:B ranging from 0.02-0.44) in surface soils across a large gradient of ecosystem
253 types (44). Rapid incorporation of labeled substrate pulses into the phospholipids of
254 Betaproteobacteria also support the view that r-strategist fractions of the community are
255 competitive LMWOS incorporators (39). In accordance with this paradigm, our growth data
256 illustrated faster growth (Table 1) and higher substrate depletion rates (Fig. 3) by the two
257 Betaproteobacteria compared to the ascomycete. Our growth rates in defined media were within
258 the range of reported specific growth rates from intact soils (45-47). *P. solitsugae* grew faster in
259 this defined media than in soil extract from the field site of origin (0.29 vs 0.17 hr^{-1}) (32),
260 indicating that estimated growth rates for these isolates are likely to be lower in intact soils.
261 Lowered rates in more chemically complex soil solution are potentially due to induced stress
262 from other compounds present (e.g., antibiotics) or reduced bioavailability of LMWOS.
263 Evaluations of fungal-to-bacterial dominance in long-term experiments (48) and laboratory
264 assessments (44) have shown increased fungal response to high quality plant litter inputs,
265 complicating the broad delineation that r-strategists (such as Betaproteobacteria) are the first
266 responders to LMWOS inputs. Fungal species, such as *P. spinulosum*, may have competitive
267 advantages in a complex soil environment other than growth rate, including the ability to explore
268 more soil pore volume for available substrates (49). Faster growth is often assumed to come at
269 the expense of CUE (24), representing a tradeoff between the ability to rapidly compete for
270 available substrates and the efficiency of their incorporation into new cellular material.
271 Our estimates of cumulative CUE (Fig. 4G-I) did not align with theories of lower CUE
272 from faster growing bacterial phylogenies (26, 50). The CUE estimates (0.54-0.84), calculated
273 using biomass and CO_2 datasets collected with population cultures of each organism, were about
274 the same as or higher than the average estimate from soil microbial communities of ~0.55 (24)

and higher than CUE measurements taken at larger temporal or spatial scales, which range from ~0.2-0.5 (51, 52). Though higher values are expected for measurements at the population level (CUE_p) (21), our observations approached the theoretical maximum efficiency (0.88) of reduced compounds (19, 53). Lower CUEs in soil may result from increased biomass maintenance costs, nutrient limitation, and resource limitation (24, 54, 55), though certain discrepancies may be a result of methodological considerations (56). The defined media used in this experiment was not nutrient limited and all carbon substrates were in monomer form, likely providing favorable conditions for organisms to grow at their maximum potential efficiency. The correlation between growth rate and CUE has been shown to be complex and sometimes inconsistent (50). It was not therefore surprising that we did not observe any correlation between growth rate and CUE under these growth conditions. Furthermore, as described in a revised trait-based theory of microbial life history (Y-A-S), high growth rate may result from any ecological strategy paired with the right context and does not necessarily entail a tradeoff with yield (57).

LMWOS utilization: Evidence for substrate co-utilization. Microbial substrate utilization preferences are thought to arise from the competitive advantage substrates offer to whichever ecological strategy is employed by the organism. Termed carbon catabolite repression, most microbes sequentially move through LMWOS that offer higher potential growth rates or yields (58, 59). Heterotrophic microorganisms have been known to deviate from sequential, diauxic growth when diverse substrates are present at low concentrations (34) and new exometabolomic work has stressed substrate co-utilization as a typical phenomenon (36, 40). Here, our data also provided evidence for diauxie and co-utilization in our substrate uptake dynamics for all isolates, characterized by clustered substrate uptake patterns with overlapping usage windows (Fig. 1).

298 The growth of the bacterial isolate, *P. solitsugae*, provided the strongest case for
299 clustered substrate co-utilization, with broader substrate usage across the growth curve and more
300 distinct cluster dynamics than the other two isolates (Fig. 1C-D). By comparison, *R. pickettii* and
301 *P. spinulosum*, had more tightly grouped substrate clusters centered around the midpoint of total
302 carbon depletion from the media (Fig. 1A-B, Fig. 1E-F, Fig. 3D, 3F). High resolution sampling
303 along the growth curve may be needed to observe lags in growth, which would be indicative of
304 changes in membrane transport system regulation as the population switched to a new cluster of
305 substrates, such as in the case of *P. solitsugae*. Thus far, we have assumed that growth of these
306 microbial populations relied on a relatively homogeneous metabolism within the population at
307 any point in time. However, there could be anabolic heterogeneity within the population, as has
308 been shown with single-cell studies (60), and this fluctuating heterogeneity could explain some
309 of our divergence in substrate uptake between isolates. Phenotypic heterogeneity in terms of
310 metabolism has been observed in clonal *Saccharomyces cerevisiae* populations under nutrient-
311 limited conditions and is likely common in microbial populations (61, 62). Regardless of the
312 mechanism leading to both diauxic and co-utilization patterns during substrate uptake, prior
313 work with a marine heterotroph, *Pseudoalteromonas haloplanktis*, as well as two common soil
314 pseudomonads indicate that potential substrate-specific growth rate may still dictate substrate
315 preference (36, 40).
316 The ordering of LMWOS utilization could arise from the interplay between the
317 expression of membrane transporter systems, system affinity, and the metabolic processing rates
318 of the substrate inside the cell (17). We found substantial uptake of organic acids predominantly
319 in the initial cluster (Cluster A) for both bacteria, but not for the fungal isolate (Fig. 2). These
320 data are consistent with prior observations of the earlier uptake of organic acids compared to

sugars and amino acids from soil solution by intact soil communities (4, 15), implying that this phenomenon is driven by fast-responding, bacterial populations similar to the two Betaproteobacteria examined in this study. Early organic acid uptake at the population-level in these bacteria may be due to the need for reducing equivalents from the metabolism of citric acid cycle intermediates when initiating growth, albeit not all organic acids (e.g., gluconate, formate, pyruvate) feed into the TCA cycle directly. The LMWOS substrate uptake ordering may also be dictated by transporter system expression more than the affinity of the different transporter systems. Our uptake rates (Fig. 3A-B) were comparable with the lowest rates measured for other soil bacterial species (40) and 2-3 orders of magnitude below modeled maximum substrate uptake rates (<74.9 μM substrate (mg C biomass)$^{-1}$ hr^{-1} vs. 33,000 μM substrate (mg C biomass)$^{-1}$ hr^{-1}) (63). Fungal uptake rates were substantially lower than bacterial uptake rates (Fig. 3C), potentially due to either lower transporter affinities or lower expression, or both.

NOSC as a predictor of substrate preferences and use efficiencies. Substrate oxidation state, NOSC, stands to directly impact preferences and SUE via thermodynamic constrains on internal metabolism or energetic payoffs (19). Thermodynamic regulation of metabolic rates is typically only considered when terminal electron acceptors, such as O_2, are limiting, but there is growing support this phenomenon would also occur in carbon-limited, oxic environments (29). This regulation arises from the higher energy requirement ($\Delta G°_{Cox}$) of the oxidation half reaction as the substrate becomes more reduced (lower NOSC). The defined media used here can be inferred to be C-limited due to excess NH_4^+ supplied and since most amino acid LMWOS provide C:N at a ratio lower than biomass production demands.

Support for thermodynamic limitations from our substrate uptake observations are tenuous. We observed a negative correlation between NOSC and normalized substrate t_{50},

indicating an earlier and more rapid uptake of oxidized (NOSC ≥ 0) organic acids, but only for the two bacterial species (Fig. 2A-B). The early utilization of oxidized substrates by bacterial species was further corroborated in the labeled experiments, where we observed the appearance of $^{13}CO_2$ from LMWOSs with a higher NOSC (e.g., formate and acetate) before other labeled substrates with lower NOSC (Fig. 4D, 4E). While there can be a decoupling of substrate uptake and metabolic use in certain situations, this is a reasonable indicator of uptake. In instances where extracellular and respiration data were both present, t_{50} values were similar or respiration data was slightly delayed. For the fungal species, there was no clear trend between NOSC and the midpoint of substrate depletion (t_{50}) from unlabeled (Fig. 2C) or labeled experiments (Fig. 4F). It is unclear why there was not early uptake of more oxidized, organic acids by *P. spinulosum*, but this may reflect a metabolic strategy prioritizing sugar uptake (glucose, galactose, xylose). The potential trends we observed from unlabeled and labeled experiments for the two bacteria (Fig. 2A-B, Fig. 4D-E) provide some population-level support for whole community observations of faster uptake and mineralization of oxidized carboxylic acids (succinic acid, malic acid, formic acid) (15).

There were no significant trends supporting thermodynamic limitations on SUE (i.e., negative correlation between NOSC and SUE) (Fig. 2.4G-I). For all isolates, formate had the lowest SUE (< 0.31), which is comparable to low anabolism/catabolism estimates in soil (15). SUE estimates of the two amino acids (glycine and valine) were higher than expected for the bacterial species under a hypothesized NOSC-SUE relationship (Fig. 4G-H) but similar in magnitude to previous observations (64). These high SUE values could be due to the demand for direct incorporation into proteins during rapid growth (65, 66). For the bacterial isolates, the disconnect between the overall relationship between substrate respiration dynamics and SUE

(Fig. 4D, 4E) and the lack of a significant relationship between NOSC and SUE (Fig. 4G, 4H) may reflect a stronger control by metabolic entry points of the chosen LMWOS traced (39, 64, 66). The low SUE estimates for formate, for example, may be a result of the limited metabolic entry points for formate-derived carbon, which is assimilated by heterotrophs typically after conversion to CO_2 by formate dehydrogenases (67, 68). Thus, formate utilization by these three isolates represents heterotrophic CO_2 fixation via anaplerosis and, while still a significant route of C utilization (69), comprises a drastically different metabolic usage than the assimilation of the other labeled carbon substrates in organic form. While used previously in assessments of NOSC and SUE relationships (15), the distinct metabolic entry pathway for formate and inherently low incorporation of C via anaplerosis by heterotrophs (69) may be driving observed correlations between NOSC and SUE. Any future assessments of substrate NOSC should include alternative oxidized substrates (e.g., oxalate) that are known to be incorporated directly (70).

The lack of consensus across all three isolates implies NOSC is not a reliable parameter for predicting substrate utilization patterns or SUE. While predicted relationships between NOSC and LMWOS t_{50} from bacterial observations agree with those produced in other stable isotope tracer experiments in soils (15), the population-level trends we observed were not strong (adj R^2 < 0.12) and not present in data from the fungal isolate (Fig. 5). It remains unknown if the earlier use of oxidized organic acids than other substrates by these bacteria, whether a result of metabolism regulation or transporter affinity, would still be apparent with unequal substrate concentrations as is typical in soil solution (32). Previous attempts to connect the processing of LMWOS in soil to inherent chemical properties, such as C:N or molecular weight, have provided inconclusive results (71). Similarly, our results stress that a fuller understanding of the internal

biochemical pathways, and not substrate NOSC alone, is necessary to predict LMWOSs cycling in soils (66).

Tracking the transformation of LMWOSs into soil carbon pools with longer turnover times requires knowledge of the principles governing microbial uptake and metabolic transformation. Many current conceptual frameworks for understanding these processes revolve around tradeoffs between microbial growth rate and CUE and the energy content of the LMWOS. Clustered substrate utilization was observed for all three microbial isolates cultured, indicating metabolic co-utilization of LMWOSs during growth. We only found potential trends ($p < 0.05$) supporting the preferential uptake of LMWOSs with higher NOSC for the two Betaproteobacteria, though variability was high and the overall effect of NOSC was small. We found no support for relationships between NOSC and SUE, highlighting the need to understand better the intracellular metabolism of LMWOS-carbon during growth. Despite community-level observations depicting a negative relationship between NOSC and half-life in solution as well as NOSC and SUE, our findings suggest that these observations may reflect the primary involvement of rapidly responding bacterial populations and that extrapolation of these results to other aerobic contexts should be approached with caution. Our ecophysiological approach, probing the carbon usage of diverse LMWOSs at realistic soil solution concentrations, presents a platform to test foundational relationships between LMWOS identity and substrate use across a range of microbial phylogenetic diversity and environmental contexts.

Materials and Methods

Microbial isolation and characterization. All strains were isolated from both field moist Oa and B horizons found under a hemlock-dominated stand in Arnot Forest, New York,

412 USA. Three microbial strains were chosen from a library originally isolated using soil-
413 extractable, solubilized organic matter (SESOM). All SESOM was derived from the Oa horizon.
414 The extract was created using a modified water extraction (72), involving the suspension of 40 g
415 of field-moist Oa horizon with 200 mL of 18.2 MΩ-cm water. Samples were shaken end-to-end
416 for 1 hour at room temperature and then left to settle. After 24 hours, the solution was
417 sequentially filtered through 1.6 μm GF/A, 0.45 μm polyethersulfone (PES), and then filter-
418 sterilized using 0.2 μm PES filters. Enrichment steps were conducted using fresh soil shaken
419 with DI water (1:10 ratio) for 1 hour and then left standing for 24 hours at room temperature.
420 Enrichments were serially diluted using Winogradsky salts (73) and a 100 μL sample was then
421 spread onto agar plates (15 g/L) created with SESOM as the sole C-source (denoted "N") and
422 with the addition of streptomycin and Rose Bengal (denoted "RB"). All plates were incubated in
423 the dark at room temperature for 3-14 days. Colonies were chosen and re-streaked 3 times before
424 growth was checked in SESOM liquid culture (2x dilution). Further details about the chemical
425 characterization of SESOM and the growth of *Paraburkholderia solitsugae* in SESOM have
426 previously been reported (32).

427 Isolates B3N, B1N, and Oa1RB were chosen based on growth rates in defined media and
428 characterized using a combination of genomic approaches. Both bacterial species were identified
429 using genomic DNA as discussed previously in Cyle et al., 2020. Briefly, genomic DNA was
430 extracted from pelleted cells and submitted to the Cornell University Sequencing Facility for
431 sequencing using three multiplexed runs of llumina MiSeq Nano (2 x 250 bp). Fungal
432 identification was conducted using ITS1F (CTTGGTCATTTAGAGGAAGTAA) and ITS4
433 primers (TCCTCCGCTTATTGATATGC) (74). *Paraburkholderia solitsugae* was extensively
434 characterized in prior works (32, 75). The other two isolates chosen are referred to by the species

name with which they have the highest similarity (Table S1). Isolate B3N was found to be most related to *Ralstonia pickettii*, a rod-shaped Betaproteobacterium (76), while isolate Oa1RB was found to be most related to *Penicillium spinulosum*, an ascomycete (77).

Media preparation and culturing conditions. All experiments were conducted in batch cultures using acid-washed and autoclaved 125-mL Erlenmeyer flasks using three biological replicates per treatment. Incubating flasks were maintained at room temperature on a shaker at 150 rpm. Defined media was prepared based on potential carbon substrates utilized by *P. solitsugae* during growth in SESOM (32). To assess the relative role of NOSC on utilization profiles and use efficiencies of each substrate, all carbon substrates were added to the media at equimolar concentration (25 μM each). Substrates included three sugars (glucose, galactose, xylose), 20 amino acids (alanine, arginine, asparagine, citrulline, cysteine, glutamate, glutamine, glycine, histidine, lysine, methionine, ornithine, isoleucine, leucine, lysine, phenylalanine, proline, serine, threonine, tryptophan, valine) and 10 organic acids (acetate, α-ketoglutarate, citrate, formate, gluconate, lactate, malate, oxalate, pyruvate, succinate). The defined medium was filter-sterilized and subsequently supplemented with 1.68 mM NH_4Cl, 0.12 mM KH_2PO_4, 1x Wolfe's vitamins and 1x Wolfe's minerals solutions (78), and pH-adjusted to pH 4.5. The nutrient media was prepared in two different manners: (1) with all unlabeled substrates and (2) with a single substrate isotopically labeled with the remaining unlabeled substrates to allow the tracking of labeling into respired CO_2 and into biomass.

Species were individually cultured in unlabeled defined media until exponential growth phase and then a sample of this culture was used to inoculate treatment flasks for experimental trials. For trials with bacterial species (*R. pickettii, P. solitsugae*), this involved overnight culturing and monitoring of growth using optical density at 595 nm (OD_{595}) followed by

458 inoculation of 50 mL treatment flasks with less than a 250 µL subsample (theoretical starting
459 OD_{595} ~ 0.0005). For trials with *P. spinulosum*, biomass measurements were made using
460 destructive sampling of biological replicates of starter flasks (n = 3 per time point), filtration
461 through 0.2 µm PES filters, and mass determination after drying at 55°C for 1 hour. At roughly
462 the inflection point of the growth curve, a single flask was sonicated for 5 minutes and 100 µL
463 volumes were used to initiate all treatments. All culturing work was conducted in a laminar flow
464 hood using aseptic technique, sterile filter-pipette tips, and with negative controls (n = 3) to
465 ensure sterility was maintained.

466 **Unlabeled growth trials. (I) Time-resolved metabolic footprinting sampling.** For
467 determining substrate utilization profiles, growth trials were conducted solely using the defined
468 media with unlabeled substrates. A growth trial was initiated for each isolate as described above,
469 with sufficient replicates to allow at least four destructive sampling time points across the
470 organism's growth curve. For bacterial species (*R. pickettii*, *P. solitsugae*), destructive sampling
471 consisted of centrifugation of ~40 mL of the culture at 10,000 x *g* for 10 minutes.
472 Supernatant was decanted and filtered through 0.2 µm PES filters. For the fugal species (*P.*
473 *spinulosum*), the entire culture of ~50 mL was filtered through 0.2 µm PES filters. All samples
474 were immediately allocated into 2-mL centrifuge tubes and stored frozen (-20°C) until
475 exometabolomics analysis. All filtered samples were analyzed using a Shimadzu TOC-V_{CPN} for
476 non-purgeable organic carbon (referred to as total organic carbon – TOC) and total nitrogen (TN)
477 using a 2% acidification (0.2 M HCl) and 1:30 min sparge time using high temperature (720^{o}C)
478 catalytic (Pt) oxidation.

479 **(II) Targeted analytes via LC-HRMS.** Stored samples were thawed and prepared for
480 immediate analysis using liquid chromatography coupled with high resolution mass spectrometry

(LC-HRMS) as described in (32). Briefly, samples were analyzed using a Thermo Scientific Dionex Ultimate 3000 liquid chromatography system connected to a Q Exactive orbitrap mass spectrometer. A reversed-phase approach using a C18 column and negative electrospray ionization (79, 80) as well as a hydrophilic interaction approach using polarity switching (81) was used to quantitate substrate concentrations in the extracellular media. Quality control checks were run every 10 samples with a 30% standard deviation limit. All data was processed using an internally constructed template within Thermo Scientific Xcalibur 3.0 Quan browser using standards of all identified compounds run between 0-25 μM. Reliable data on three compounds not intentionally added to the minimal media (fumarate, cystine, and homoserine) have been included in all analyses.

(III) Targeted analytes via ^{1}H NMR. Samples were analyzed using proton nuclear magnetic resonance spectrometry (^{1}H NMR) to capture a select group of sugars and organic acids from the media that could not be quantified during some LC-HRMS analytical runs (glucose, galactose, xylose, acetate, formate, oxalate, valine). Methods used have been previously reported for extracted soil solutions (32, 72, 82). Briefly, 35-40 mL samples of frozen extracellular media were concentrated by lyophilizing the sample and reconstituting to a smaller, final volume of 500 μL. Reconstitution involved 300 μL of 18.2 MΩ-cm water and buffered to pH of 7.0 using an addition of 200 μL of sodium hydrogen phosphate (0.1 mM, pH 7.0) made with 25% D_2O (vol/vol) to supply a lock signal and containing 1 mM sodium 3-trimethylsilyl-[2,2,3,3,-D_4]-1 propionic acid (TMSP) to provide spectral referencing at a final concentration of 0.4 mM. All spectra were collected at 500 MHz at room temperature on a Bruker AV 500 operated using Bruker TopSpin 3.5.7 using a 10% D_2O and water peak suppression program (noesygppr1d) with 32 scans/sample and a 5-s relaxation delay for a total of 256 transients.

Previously described spectral processing methods and integral regions (32) were used on all samples. Areas under the curve were normalized to initial media values for each experiment and used for depletion model fitting. No reliable sugar data was able to be collected, though in some cases valine, acetate, and formate were able to be modeled and are included in analyses.

(IV) Curve fits for microbial growth and substrate depletion analysis. Microbial growth was modeled using R 3.6.0 (83) using the nls.multstart package (84). Microbial growth was modeled in terms of biomass (mg L^{-1}) to ensure equivalent comparison of growth rates between bacterial isolates, which were originally monitored in terms of OD_{595}, and the fungal isolate, which was originally monitored in terms of biomass. Conversion from OD_{595} to mg L^{-1} for the bacterial species was conducted using a biomass conversion factor (k – mg L^{-1}, Table 1), determined on and OD unit basis using biomass data collected at stationary phase during the labeled growth trials. Growth was modeled using a reparametrized Gompertz equation (Eq. 1) (85) on untransformed biomass data to allow extraction of parameters with biological meaning and for visualization purposes,

$$y = Ae^{-e^{(\frac{\mu e}{A}(\lambda - t)+1)}} \quad (1)$$

where y is average biomass data (mg L^{-1}), A is the stationary phase asymptote of the growth curve (mg L^{-1}), t is time (h), μ is the specific growth rate (h^{-1}), λ is the lag time (h^{-1}). A secondary fitting approach was employed using the growthrates package (86) to produce normalized estimates of specific growth rate (μ, hr^{-1}) from average biomass data, readily allowing comparisons with literature values while avoiding biases from estimates of biomass from initial cell density (N_0) (87).

Substrate depletion was analyzed based on pattern clustering, nonlinear modeling, and calculations of maximum depletion rate. Clusters of substrate depletion were identified for each

527 isolate using a k-means approach specifically suited for comparing trajectories. Substrate
528 depletion observations, normalized to measured initial media concentrations, were analyzed
529 using the kml package (88) in R 3.6.0 (83). Clusters were iteratively analyzed ensuring clusters
530 of sufficient size (10%) and maximizing the Calinski-Harabanz index (89). Model fits of
531 substrate depletion data and extracellular TOC were created for individual biological replicates
532 using the nls.multstart package (84) as described previously (32, 40, 90). A nonlinear modeling
533 approach (Eq. 2) allowed the fitting of a 4-point sigmoidal curve using the following equation:

534 $$y = \frac{a}{1 + e^{\frac{t - t_{50}}{w}}} + o \qquad (2)$$

535 where *y* represented either concentration data (μM) or in some cases was normalized relative to
536 initial conditions (0-1) and *t* represents time (h). The four parameters produced during the fitting
537 procedure relate to the amplitude of substrate depletion (*a*, μM or unitless), the midpoint of
538 depletion (t_{50}, h), the width of the concentration decrease (*w*, h), and the offset or predicted final
539 value of substrate remaining in extracellular media (*o*, μM or unitless). For visualization and
540 comparison purposes, the midpoint of depletion (t_{50}) has been chosen as the point to assess
541 substrate uptake ordering. The width parameter has been modified in all figures to show a wide
542 usage window towards capturing substrate use overlap. The usage window extends from 10% of
543 total substrate utilization or where y = [(*a*-*o*) x 0.9] as well as the time at which 90% of total
544 substrate utilization has occurred or where y = [(*a*-*o*) x 0.1]. In some cases, no fit was applied
545 due to insufficient data or indications that a sigmoidal fit was not the appropriate model.
546 Maximum depletion rate was determined by taking the differential of the modeled substrate
547 depletion curve and calculating the rate at the inflection point (t_{50}) (40) and expressing that value
548 as a rate normalized in terms of cell dry weight (μmol h^{-1} mg_{CDW}^{-1}). In some cases, the midpoint
549 of depletion, t_{50}, has been normalized to the stationary phase sampling time (0-1) for easier

comparison across isolate growth curves. All two-group comparisons between compound classes were conducted using a Welch's t-test and the relationship between NOSC and normalized t_{50} was assessed using linear regression.

Labeled growth trials. (I) Respiration sampling during growth. Growth trials were conducted for each isolate using labeled substrates (> 98% ^{13}C, 99% ^{15}N, Cambridge Isotope Laboratories, Inc.) to track C into ^{13}C labeled microbial biomass as well as respired $^{13}CO_2$. Five labeled treatments were chosen to span low molecular weight compound classes (sugar, organic acid, amino acid) as well as nominal oxidation states of carbon (-0.8 – 2). Substrates included a sugar (glucose, NOSC = 0), two organic acids (acetate, NOSC = 0 and formate, NOSC = 2), and two amino acids (glycine, NOSC = 1 and valine, NOSC = -0.8). Each labeled treatment contained the labeled substrate as well as the remaining unlabeled 33 substrates.

Culturing was conducted as described previously except rubber septa were fitted after inoculation to seal off the headspace of the flask. At intervals during growth, 250 μL headspace gas samples were taken using a 500 μL gastight syringe. Gas samples were then injected into pre-evacuated, and helium (He) filled 2 mL glass crimp vials sealed with a PTFE/butyl septum. The quantity of $^{12}CO_2$ (m/z 44) and $^{13}CO_2$ (m/z 45) were measured using gas chromatography-mass spectrometry using a Shimadzu GCMS-QP2010S equipped with a Carboxen 1010 PLOT column and ultra-high purity He (Airgas, Inc.) as the carrier gas using previously described protocols (18, 91). Samples were run within 24 hours and each sample run was accompanied by standards ranging from 0-17,700 ppm created using CO_2 (Airgas, Inc.). No purging was conducted in between sampling points, so all data represents cumulative buildup of CO_2 in the headspace. All values are displayed as CO_2-C (% of addition). This was calculated by first subtracting natural abundance $^{13}CO_2$ determined using the unlabeled control treatments. This

enriched $^{13}CO_2$ value was converted to mg ^{13}C and divided by the amount of labeled substrate supplied in the treatment. Cumulative CO_2 curves were modeled using a modified version of equation 2 with the numerator altered to $[-(x - t_{50})]$ to invert the 4-point sigmoidal fit for the hypothetical curve of mirrored CO_2 release. The offset parameter (o) was also set to 0 for this scenario.

(II) Biomass harvest and isotopic measurements. At the beginning of stationary phase, isolate biomass was destructively harvested from all culture flasks. Destructive sampling was conducted as described for unlabeled growth trials. All biomass, whether separated using a filter or centrifugation, was washed using 5 mL of C-free 1x Wolfe's minerals solutions. A portion of separated biomass was then submitted to the Cornell Stable Isotope Laboratory for combustion analysis using a Thermo Delta V isotope ratio mass spectrometer (IRMS) interfaced to a NC2500 elemental analyzer.

(III) Calculations and data visualization. All post-processing was conducted in R 3.6.0 (83) using the tidyverse package (92), the RColorBrewer package (93), and the cowplot package (94). The SUE (Eq. 3) and CUE (Eq. 4) values were both estimated by combining the isotopic data for CO_2 and biomass as evaluated at stationary phase. The SUE was calculated as:

$$SUE = \frac{^{13}C_{MBIO}}{^{13}C_{CO_2} + {}^{13}C_{MBIO}} \quad (3)$$

where $^{13}C_{CO2}$ (mg) and $^{13}C_{MBIO}$ (mg) was determined for each replicate after subtraction of the average natural abundance ^{13}C in both pools using atom percent ^{13}C values from unlabeled treatments. The CUE was calculated similarly but using the total values of C.

$$CUE = \frac{^{12}C_{MBIO} + {}^{13}C_{MBIO}}{(^{12}C_{CO_2} + {}^{13}C_{CO_2}) + (^{12}C_{MBIO} + {}^{13}C_{MBIO})} \quad (4)$$

Statistical comparisons between treatments for dependent variables (t_{50}, SUE) were analyzed first using ANOVA and then subsequent multiple comparison tests were conducted using Tukey's HSD. Correlations were assessed using linear regression.

Data Availability. The genome assembly for strain B1N (*Paraburkholderia solitsugae*) and strain B3N (*Ralstonia pickettii*) can be accessed via the NCBI portal using the BioProject accession numbers PRJNA590275. The ITS sequence for strain Oa1RB (*Penicillium spinulosum*) can be accessed via the NCBI GenBank portal using accession numbers MZ375756. Metabolomics data have been deposited to the EMBL-EBI MetaboLights database (DOI: 10.1093/nar/gkz1019, PMID:31691833) with the identifier MTBLS3558 (95).

Acknowledgements

Graduate financial support for K.T.C. was provided by the College of Agriculture and Life Sciences at Cornell University. Partial graduate financial support and funding was provided by the Cornell University Program in Cross-Scale Biogeochemistry and Climate, which is supported by NSF-IGERT and the Atkinson Center for a Sustainable Future. Postdoctoral support for A.R.K. was provided by a National Science Foundation CAREER Grant (award # 1653092) awarded to L.A. This work was also supported by the AFRI Education and Workforce Development Program, grant no. 2019-67011-29513, from the U.S. Department of Agriculture, National Institute of Food and Agriculture. We thank Roland Wilhelm, Dan Buckley, and Martínez Research Group members for helpful revisions to the manuscript. Sequencing was performed by the Biotechnology Resource Center (BRC) Genomics Facility at Cornell University (*http://www.biotech.cornell.edu/brc/genomics-facility*). ^{1}H NMR experiments were performed at the Cornell University NMR facility in the Department of Chemistry and Chemical Biology.

References

1. Marschner B, Kalbitz K. 2003. Controls of bioavailability and biodegradability of dissolved organic matter in soils. Geoderma 113:211-235.

2. Roth V-N, Lange M, Simon C, Hertkorn N, Bucher S, Goodall T, Griffiths RI, Mellado-Vázquez PG, Mommer L, Oram NJ. 2019. Persistence of dissolved organic matter explained by molecular changes during its passage through soil. Nature Geoscience 12:755-761.

3. van Hees PAW, Jones DL, Finlay R, Godbold DL, Lundstomd US. 2005. The carbon we do not see - the impact of low molecular weight compounds on carbon dynamics and respiration in forest soils: a review. Soil Biology & Biochemistry 37:1-13.

4. Glanville H, Rousk J, Golyshin P, Jones D. 2012. Mineralization of low molecular weight carbon substrates in soil solution under laboratory and field conditions. Soil Biology and Biochemistry 48:88-95.

5. Jones DL, Edwards AC. 1998. Influence of sorption on the biological utilization of two simple carbon substrates. Soil Biology & Biochemistry 30:1895-1902.

6. Sasse J, Martinoia E, Northen T. 2018. Feed Your Friends: Do Plant Exudates Shape the Root Microbiome? Trends in Plant Science 23:25-41.

7. Jones D, Dennis P, Owen A, Van Hees P. 2003. Organic acid behavior in soils–misconceptions and knowledge gaps. Plant and Soil 248:31-41.

8. Chagas FO, de Cassia Pessotti R, Caraballo-Rodriguez AM, Pupo MT. 2018. Chemical signaling involved in plant–microbe interactions. Chemical Society Reviews 47:1652-1704.

9. Kuzyakov Y. 2006. Sources of CO2 efflux from soil and review of partitioning methods. Soil Biology and Biochemistry 38:425-448.

10. Sokol NW, Sanderman J, Bradford MA. 2019. Pathways of mineral-associated soil organic matter formation: Integrating the role of plant carbon source, chemistry, and point of entry. Global Change Biology 25:12-24.

11. Fischer H, Ingwersen J, Kuzyakov Y. 2010. Microbial uptake of low-molecular-weight organic substances out-competes sorption in soil. European Journal of Soil Science 61:504-513.

12. Glanville H, Hill P, Schnepf A, Oburger E, Jones D. 2016. Combined use of empirical data and mathematical modelling to better estimate the microbial turnover of isotopically labelled carbon substrates in soil. Soil Biology and Biochemistry 94:154-168.

13. Bradford MA, Keiser AD, Davies CA, Mersmann CA, Strickland MS. 2013. Empirical evidence that soil carbon formation from plant inputs is positively related to microbial growth. Biogeochemistry 113:271-281.

14. Brant JB, Sulzman EW, Myrold DD. 2006. Microbial community utilization of added carbon substrates in response to long-term carbon input manipulation. Soil Biology & Biochemistry 38:2219-2232.

15. Gunina A, Smith AR, Kuzyakov Y, Jones DL. 2017. Microbial uptake and utilization of low molecular weight organic substrates in soil depend on carbon oxidation state. Biogeochemistry 133:89-100.

16. Jones DL, Hodge A. 1999. Biodegradation kinetics and sorption reactions of three differently charged amino acids in soil and their effects on plant organic nitrogen availability. Soil Biology and Biochemistry 31:1331-1342.

17. Hill PW, Farrar JF, Jones DL. 2008. Decoupling of microbial glucose uptake and mineralization in soil. Soil Biology and Biochemistry 40:616-624.

18. Barnett SE, Youngblut ND, Koechli CN, Buckley DH. 2021. Life history strategies explain bacterial activity in the soil carbon cycle. bioRxiv doi:10.1101/2021.03.19.436178:2021.03.19.436178.

19. Gommers PJF, Vanschie BJ, Vandijken JP, Kuenen JG. 1988. Biochemical limits to microbial-growth yields - an analysis of mixed substrate utilization. Biotechnology and Bioengineering 32:86-94.

20. Roels J. 1980. Application of macroscopic principles to microbial metabolism. Biotechnology and Bioengineering 22:2457-2514.

21. Geyer KM, Kyker-Snowman E, Grandy AS, Frey SD. 2016. Microbial carbon use efficiency: accounting for population, community, and ecosystem-scale controls over the fate of metabolized organic matter. Biogeochemistry doi:10.1007/s10533-016-0191-y:1-16.

22. Li J, Wang G, Allison SD, Mayes MA, Luo Y. 2014. Soil carbon sensitivity to temperature and carbon use efficiency compared across microbial-ecosystem models of varying complexity. Biogeochemistry 119:67-84.

23. Liang C, Schimel JP, Jastrow JD. 2017. The importance of anabolism in microbial control over soil carbon storage. Nature Microbiology 2:17105.

24. Manzoni S, Taylor P, Richter A, Porporato A, Agren GI. 2012. Environmental and stoichiometric controls on microbial carbon-use efficiency in soils. New Phytologist 196:79-91.

25. Roller BRK, Schmidt TM. 2015. The physiology and ecological implications of efficient growth. ISME J 9:1481-1487.

26. Roller BRK, Stoddard SF, Schmidt TM. 2016. Exploiting rRNA operon copy number to investigate bacterial reproductive strategies. Nature Microbiology 1:16160.

27. Kleber M. 2010. What is recalcitrant soil organic matter. Environmental Chemistry 7:320-332.

28. LaRowe DE, Van Cappellen P. 2011. Degradation of natural organic matter: A thermodynamic analysis. Geochimica Et Cosmochimica Acta 75:2030-2042.

29. Garayburu-Caruso VA, Stegen JC, Song H-S, Renteria L, Wells J, Garcia W, Resch CT, Goldman AE, Chu RK, Toyoda J, Graham EB. 2020. Carbon Limitation Leads to Thermodynamic Regulation of Aerobic Metabolism. Environmental Science & Technology Letters 7:517-524.

30. Graham EB, Tfaily MM, Crump AR, Goldman AE, Bramer LM, Arntzen E, Romero E, Resch CT, Kennedy DW, Stegen JC. 2017. Carbon Inputs From Riparian Vegetation Limit Oxidation of Physically Bound Organic Carbon Via Biochemical and Thermodynamic Processes. Journal of Geophysical Research: Biogeosciences 122:3188-3205.

31. Stegen JC, Johnson T, Fredrickson JK, Wilkins MJ, Konopka AE, Nelson WC, Arntzen EV, Chrisler WB, Chu RK, Fansler SJ, Graham EB, Kennedy DW, Resch CT, Tfaily M, Zachara J. 2018. Influences of organic carbon speciation on hyporheic corridor biogeochemistry and microbial ecology. Nature Communications 9:585.

32. Cyle KT, Klein AR, Aristilde L, Martínez CE. 2020. Ecophysiological Study of *Paraburkholderia* sp. Strain 1N under Soil Solution Conditions: Dynamic Substrate

730 Preferences and Characterization of Carbon Use Efficiency. Applied and Environmental
731 Microbiology 86:e01851-20.
732 33. Egli T. 1995. The Ecological and Physiological Significance of the Growth of
733 Heterotrophic Microorganisms with Mixtures of Substrates, p 305-386. *In* Jones JG (ed),
734 Advances in Microbial Ecology doi:10.1007/978-1-4684-7724-5_8. Springer US, Boston,
735 MA.
736 34. Kovárová-Kovar K, Egli T. 1998. Growth kinetics of suspended microbial cells: from
737 single-substrate-controlled growth to mixed-substrate kinetics. Microbiology and
738 molecular biology reviews 62:646-666.
739 35. Kukurugya MA, Mendonca CM, Solhtalab M, Wilkes RA, Thannhauser TW, Aristilde L.
740 2019. Multi-omics analysis unravels a segregated metabolic flux network that tunes co-
741 utilization of sugar and aromatic carbons in Pseudomonas putida. Journal of Biological
742 Chemistry 294:8464-8479.
743 36. Perrin E, Ghini V, Giovannini M, Di Patti F, Cardazzo B, Carraro L, Fagorzi C, Turano
744 P, Fani R, Fondi M. 2020. Diauxie and co-utilization of carbon sources can coexist
745 during bacterial growth in nutritionally complex environments. Nature Communications
746 11:3135.
747 37. Song H-S, Stegen JC, Graham EB, Lee J-Y, Garayburu-Caruso VA, Nelson WC, Chen
748 X, Moulton JD, Scheibe TD. 2020. Representing Organic Matter Thermodynamics in
749 Biogeochemical Reactions via Substrate-Explicit Modeling. Frontiers in Microbiology
750 11.

751 38. Tang JY, Riley WJ. 2013. A total quasi-steady-state formulation of substrate uptake
752 kinetics in complex networks and an example application to microbial litter
753 decomposition. Biogeosciences 10:8329-8351.
754 39. Gunina A, Dippold MA, Glaser B, Kuzyakov Y. 2014. Fate of low molecular weight
755 organic substances in an arable soil: From microbial uptake to utilisation and
756 stabilisation. Soil Biology and Biochemistry 77:304-313.
757 40. Erbilgin O, Bowen BP, Kosina SM, Jenkins S, Lau RK, Northen TR. 2017. Dynamic
758 substrate preferences predict metabolic properties of a simple microbial consortium.
759 BMC bioinformatics 18:57.
760 41. Zhalnina K, Louie KB, Hao Z, Mansoori N, da Rocha UN, Shi S, Cho H, Karaoz U,
761 Loqué D, Bowen BP, Firestone MK, Northen TR, Brodie EL. 2018. Dynamic root
762 exudate chemistry and microbial substrate preferences drive patterns in rhizosphere
763 microbial community assembly. Nature Microbiology 3:470-480.
764 42. Fierer N, Bradford MA, Jackson RB. 2007. Toward an ecological classification of soil
765 bacteria. Ecology 88:1354-1364.
766 43. Waring BG, Averill C, Hawkes CV. 2013. Differences in fungal and bacterial physiology
767 alter soil carbon and nitrogen cycling: insights from meta-analysis and theoretical
768 models. Ecology Letters 16:887-894.
769 44. Soares M, Rousk J. 2019. Microbial growth and carbon use efficiency in soil: Links to
770 fungal-bacterial dominance, SOC-quality and stoichiometry. Soil Biology and
771 Biochemistry 131:195-205.

45. Blagodatskaya E, Blagodatsky S, Dorodnikov M, Kuzyakov Y. 2010. Elevated atmospheric CO2 increases microbial growth rates in soil: results of three CO2 enrichment experiments. Global Change Biology 16:836-848.

46. Blagodatskaya EV, Blagodatsky SA, Anderson T-H, Kuzyakov Y. 2009. Contrasting effects of glucose, living roots and maize straw on microbial growth kinetics and substrate availability in soil. European Journal of Soil Science 60:186-197.

47. Loeppmann S, Semenov M, Blagodatskaya E, Kuzyakov Y. 2016. Substrate quality affects microbial- and enzyme activities in rooted soil. Journal of Plant Nutrition and Soil Science 179:39-47.

48. Rousk J, Frey SD. 2015. Revisiting the hypothesis that fungal-to-bacterial dominance characterizes turnover of soil organic matter and nutrients. Ecological Monographs 85:457-472.

49. Adu JK, Oades JM. 1978. Utilization of organic materials in soil aggregates by bacteria and fungi. Soil Biology and Biochemistry 10:117-122.

50. Lipson DA. 2015. The complex relationship between microbial growth rate and yield and its implications for ecosystem processes. Frontiers in Microbiology 6.

51. Sinsabaugh RL, Moorhead DL, Xu X, Litvak ME. 2017. Plant, microbial and ecosystem carbon use efficiencies interact to stabilize microbial growth as a fraction of gross primary production. New Phytologist 214:1518-1526.

52. Spohn M, Pötsch EM, Eichorst SA, Woebken D, Wanek W, Richter A. 2016. Soil microbial carbon use efficiency and biomass turnover in a long-term fertilization experiment in a temperate grassland. Soil Biology and Biochemistry 97:168-175.

794 53. Linton JD, Stephenson RJ. 1978. A preliminary study on growth yields in relation to the
795 carbon and energy content of various organic growth substrates. FEMS Microbiology
796 Letters 3:95-98.
797 54. Malik AA, Puissant J, Goodall T, Allison SD, Griffiths RI. 2019. Soil microbial
798 communities with greater investment in resource acquisition have lower growth yield.
799 Soil Biology and Biochemistry 132:36-39.
800 55. Sinsabaugh RL, Manzoni S, Moorhead DL, Richter A. 2013. Carbon use efficiency of
801 microbial communities: stoichiometry, methodology and modelling. Ecology Letters
802 16:930-939.
803 56. Geyer KM, Dijkstra P, Sinsabaugh R, Frey SD. 2019. Clarifying the interpretation of
804 carbon use efficiency in soil through methods comparison. Soil Biology and
805 Biochemistry 128:79-88.
806 57. Malik AA, Martiny JBH, Brodie EL, Martiny AC, Treseder KK, Allison SD. 2020.
807 Defining trait-based microbial strategies with consequences for soil carbon cycling under
808 climate change. The ISME Journal 14:1-9.
809 58. Görke B, Stülke J. 2008. Carbon catabolite repression in bacteria: many ways to make the
810 most out of nutrients. Nature Reviews Microbiology 6:613-624.
811 59. Kremling A, Geiselmann J, Ropers D, de Jong H. 2015. Understanding carbon catabolite
812 repression in Escherichia coli using quantitative models. Trends in Microbiology 23:99-
813 109.
814 60. Calabrese F, Stryhanyuk H, Moraru C, Schlömann M, Wick LY, Richnow HH, Musat F,
815 Musat N. 2021. Metabolic history and metabolic fitness as drivers of anabolic
816 heterogeneity in isogenic microbial populations. Environmental Microbiology n/a.

817 61. Ackermann M. 2015. A functional perspective on phenotypic heterogeneity in
818 microorganisms. Nature Reviews Microbiology 13:497-508.
819 62. Varahan S, Laxman S. 2021. Bend or break: how biochemically versatile molecules
820 enable metabolic division of labor in clonal microbial communities. Genetics 219.
821 63. Tang J, Riley WJ. 2019. Competitor and substrate sizes and diffusion together define
822 enzymatic depolymerization and microbial substrate uptake rates. Soil Biology and
823 Biochemistry 139:107624.
824 64. Vinolas LC, Healey JR, Jones DL. 2001. Kinetics of soil microbial uptake of free amino
825 acids. Biology and Fertility of Soils 33:67-74.
826 65. Geisseler D, Horwath WR, Joergensen RG, Ludwig B. 2010. Pathways of nitrogen
827 utilization by soil microorganisms – A review. Soil Biology and Biochemistry 42:2058-
828 2067.
829 66. Knowles TDJ, Chadwick DR, Bol R, Evershed RP. 2010. Tracing the rate and extent of
830 N and C flow from 13C,15N-glycine and glutamate into individual de novo synthesised
831 soil amino acids. Organic Geochemistry 41:1259-1268.
832 67. Dijkhuizen L, Harder W. 1984. Regulation of Autotrophic and Heterotrophic Metabolism
833 in Pseudomonas oxalaticus OX1. Growth on Fructose and on Mixtures of Fructose and
834 Formate in Batch and Continuous Cultures. Microbiology 130:447-457.
835 68. Quayle J. 1961. Metabolism of C Compounds in Autotrophic and Heterotrophic
836 Microorganisms. Annual Reviews in Microbiology 15:119-152.
837 69. Braun A, Spona-Friedl M, Avramov M, Elsner M, Baltar F, Reinthaler T, Herndl GJ,
838 Griebler C. 2021. Reviews and syntheses: Heterotrophic fixation of inorganic carbon –

839 significant but invisible flux in environmental carbon cycling. Biogeosciences 18:3689-
840 3700.
841 70. Friedrich CG, Bowien B, Friedrich B. 1979. Formate and Oxalate Metabolism in
842 Alcaligenes eutrophus. Microbiology 115:185-192.
843 71. Roberts P, Stockdale R, Khalid M, Iqbal Z, Jones DL. 2009. Carbon-to-nitrogen ratio is a
844 poor predictor of low molecular weight organic nitrogen mineralization in soil. Soil
845 Biology and Biochemistry 41:1750-1752.
846 72. Liebeke M, Brozel VS, Hecker M, Lalk M. 2009. Chemical characterization of soil
847 extract as growth media for the ecophysiological study of bacteria. Applied Microbiology
848 and Biotechnology 83:161-173.
849 73. Dabek-Szreniawska M, Hattori T. 1981. Winogradsky's salts solution as a diluting
850 medium for plate count of oligotrophic bacteria in soil. The Journal of General and
851 Applied Microbiology 27:517-518.
852 74. Raja HA, Miller AN, Pearce CJ, Oberlies NH. 2017. Fungal Identification Using
853 Molecular Tools: A Primer for the Natural Products Research Community. Journal of
854 Natural Products 80:756-770.
855 75. Wilhelm RC, Cyle KT, Martinez CE, Karasz DC, Newman JD, Buckley DH. 2020.
856 Paraburkholderia solitsugae sp. nov. and Paraburkholderia elongata sp. nov., phenolic
857 acid-degrading bacteria isolated from forest soil and emended description of
858 Paraburkholderia madseniana. International Journal of Systematic and Evolutionary
859 Microbiology doi:https://doi.org/10.1099/ijsem.0.004387.
860 76. Yabuuchi E, Kosako Y, Yano I, Hotta H, Nishiuchi Y. 1995. Transfer of Two
861 *Burkholderia* and An *Alcaligenes* Species to *Ralstonia* Gen. Nov.: Proposal of *Ralstonia*

pickettii (Ralston, Palleroni and Doudoroff 1973) Comb. Nov., *Ralstonia solanacearum* (Smith 1896) Comb. Nov. and *Ralstonia eutropha* (Davis 1969) Comb. Nov. Microbiology and Immunology 39:897-904.

77. Haugland RA, Varma M, Wymer LJ, Vesper SJ. 2004. Quantitative PCR analysis of selected Aspergillus, Penicillium and Paecilomyces species. Syst Appl Microbiol 27:198-210.

78. Atlas RM. 2010. Handbook of microbiological media. CRC press.

79. Aristilde L, Reed ML, Wilkes RA, Youngster T, Kukurugya MA, Katz V, Sasaki CRS. 2017. Glyphosate-Induced Specific and Widespread Perturbations in the Metabolome of Soil Pseudomonas Species. Frontiers in Environmental Science 5:34.

80. Lu W, Clasquin MF, Melamud E, Amador-Noguez D, Caudy AA, Rabinowitz JD. 2010. Metabolomic analysis via reversed-phase ion-pairing liquid chromatography coupled to a stand alone orbitrap mass spectrometer. Analytical chemistry 82:3212-3221.

81. Klein AR, Barzen-Hanson KA, Aristilde L. 2020. A non-derivatized method for simultaneous quantitation of proteinogenic, urea-cycle, and acetylated amino acids by liquid chromatography–high-resolution mass spectrometry. Environmental Chemistry Letters 18:229-235.

82. Hochgräfe F, Wolf C, Fuchs S, Liebeke M, Lalk M, Engelmann S, Hecker M. 2008. Nitric Oxide Stress Induces Different Responses but Mediates Comparable Protein Thiol Protection in *Bacillus subtilis* and *Staphylococcus aureus*. Journal of Bacteriology 190:4997-5008.

83. R Core Team. 2019. R: A Language and Environment for Statistical Computing, R Foundation for Statistical Computing, Vienna, Austria. https://www.R-project.org/.

84. Padfield D, Matheson G. 2018. nls.multstart: Robust Non-Linear Regression using AIC Scores, https://CRAN.R-project.org/package=nls.multstart.

85. Zwietering MH, Jongenburger I, Rombouts FM, van 't Riet K. 1990. Modeling of the Bacterial Growth Curve. Applied and Environmental Microbiology 56:1875-1881.

86. Petzoldt T. 2018. growthrates: Estimate Growth Rates from Experimental Data., https://CRAN.R-project.org/package=growthrates.

87. Hall BG, Acar H, Nandipati A, Barlow M. 2013. Growth Rates Made Easy. Molecular Biology and Evolution 31:232-238.

88. Genolini C, Alacoque X, Sentenac M, Arnaud C. 2015. kml and kml3d: R Packages to Cluster Longitudinal Data. 2015 65:34.

89. Liu Y, Li Z, Xiong H, Gao X, Wu J. Understanding of Internal Clustering Validation Measures, p 911-916. *In* (ed),

90. Behrends V, Ebbels TMD, Williams HD, Bundy JG. 2009. Time-Resolved Metabolic Footprinting for Nonlinear Modeling of Bacterial Substrate Utilization. Applied and Environmental Microbiology 75:2453-2463.

91. Wilhelm RC, DeRito CM, Shapleigh JP, Madsen EL, Buckley DH. 2021. Phenolic acid-degrading Paraburkholderia prime decomposition in forest soil. ISME Communications 1:4.

92. Wickham H, Averick M, Bryan J, Chang W, McGowan LDA, François R, Grolemund G, Hayes A, Henry L, Hester J. 2019. Welcome to the Tidyverse. Journal of Open Source Software 4:1686.

93. Neuwirth E. 2014. RColorBrewer: ColorBrewer Palettes, https://CRAN.R-project.org/package=RColorBrewer.

908 94. Wilke CO. 2020. cowplot: Streamlined Plot Theme and Plot Annotations for 'ggplot2',
909 https://CRAN.R-project.org/package=cowplot.
910 95. Haug K, Cochrane K, Nainala VC, Williams M, Chang J, Jayaseelan KV, O'Donovan C.
911 2019. MetaboLights: a resource evolving in response to the needs of its scientific
912 community. Nucleic Acids Research 48:D440-D444.
913
914
915
916
917
918
919
920
921
922
923
924
925
926
927
928
929
930

Tables

Table 1. Observations and modeled growth curve fit parameters using biomass data.

	Observations			Gompertz Fit			Normalized Fit*
	k (mg L^{-1})	Final sample (h)	%C	A (mg L^{-1})	μ (h^{-1})	λ (h)	μ (h^{-1})
R. pickettii	674.23	22	43.4	76.05	21.28	12.55	0.32
P. solitsugae	387.32	24	28.9	49.80	6.44	11.75	0.29
P. spinulosum	-	120	43.9	46.36	1.63	42.35	0.04

k – biomass conversion factor, A – stationary phase asymptote, μ - specific growth rate, λ - lag time.
*Normalized approach (Hall et al., 2013).

950 **Figures**

951

952 **FIG 1** Depletion dynamics for observed LMWOS. Plots are paired by microbial isolate depicting
953 depletion dynamics (A, C, E) and usage window plots (B, D, F) for uptake clusters identified
954 using a k-means approach. Lines (A, C, E) are individual substrate uptake patterns normalized to
955 initial concentration (mean, n = 3) with the thickest line showing the mean of the cluster. All
956 points in usage window plots (B, D, F) are the mean modeled midpoints of depletion (t_{50}) plotted
957 over the growth curve of the isolate (black line). The mean midpoint of overall carbon depletion
958 is shown with a black circle. Horizontal bars around each t_{50} show the usage window (10% -
959 90% of initial concentration). All substrates are colored by cluster and listed in the legend in
960 order of increasing t_{50}. Ala, alanine; arg, arginine; asn, asparagine; cit, citrulline; cys, cysteine;
961 glu, glutamate; gln, glutamine; gly, glycine; his, histidine; lys, lysine; met, methionine; orn,
962 ornithine; ile, isoleucine; leu, leucine; lys, lysine; phe, phenylalanine; pro, proline; ser, serine;
963 thr, threonine; trp, tryptophan; val, valine; ace, acetate; akg, α-ketoglutarate; form, formate;
964 glucon, gluconate; lac, lactate; mal, malate; oxa, oxalate; pyr, pyruvate; succ, succinate.

965

966 **FIG 2** Inflection points of substrate depletion (t_{50}) normalized to stationary phase sampling time
967 as a function of substrate oxidation state (NOSC). Normalized t_{50} values are the mean of three
968 biological replicates with error bars representing standard error. Plots are paneled according to
969 microbial isolate (A, B, C) and shapes illustrate cluster affiliation as determined using k-means
970 clustering. Colors represent compound class (amino acid or organic acid).

971

972

FIG 3 Biomass-normalized maximum depletion rate (A-C) as a function of the inflection point of depletion (t_{50}) normalized to stationary phase sampling time. Values are the mean of three biological replicates with error bars representing standard error. Shapes illustrate cluster affiliation and colors represent compound class (amino acid or organic acid). The vertical dashed line depicts the normalized t_{50} of overall carbon depletion from the media. Several points were removed for visualization purposes due to high variance between biological replicates (*P. solitsugae* – isoleucine, *P. spinulosum* – cystine & succinate).

FIG 4 Respiration dynamics of ^{13}C-labeled substrates and cumulative respiration along with estimates of substrate use efficiency (SUE). Graphs are grouped vertically for the three microbial isolates and arranged in order of decreasing specific growth rate (*R. pickettii* > *P. solitsugae* > *P. spinulosum*). Panels display respiration as a function of time in the first row of panels (A-C), SUE as a function of the midpoint of respiration, t_{50}, (D-F), and SUE as a function of substrate oxidation state (G-I). The dashed vertical line in plots A-F indicates stationary phase of the overall growth curve and the sample point for determination of ^{13}C present in microbial biomass. The dashed horizontal line in plots G-I indicates the cumulative carbon use efficiency of all carbon sources. See Fig. S6 for full panel A and Table S6 for microbial biomass carbon and nitrogen composition data. Glc, glucose; Ace, acetate; Form, formate; Gly, glycine; Val, valine.

FIG 5 Summary chart outlining the results of this study and the possible implications at the community level. Created with BioRender.com.

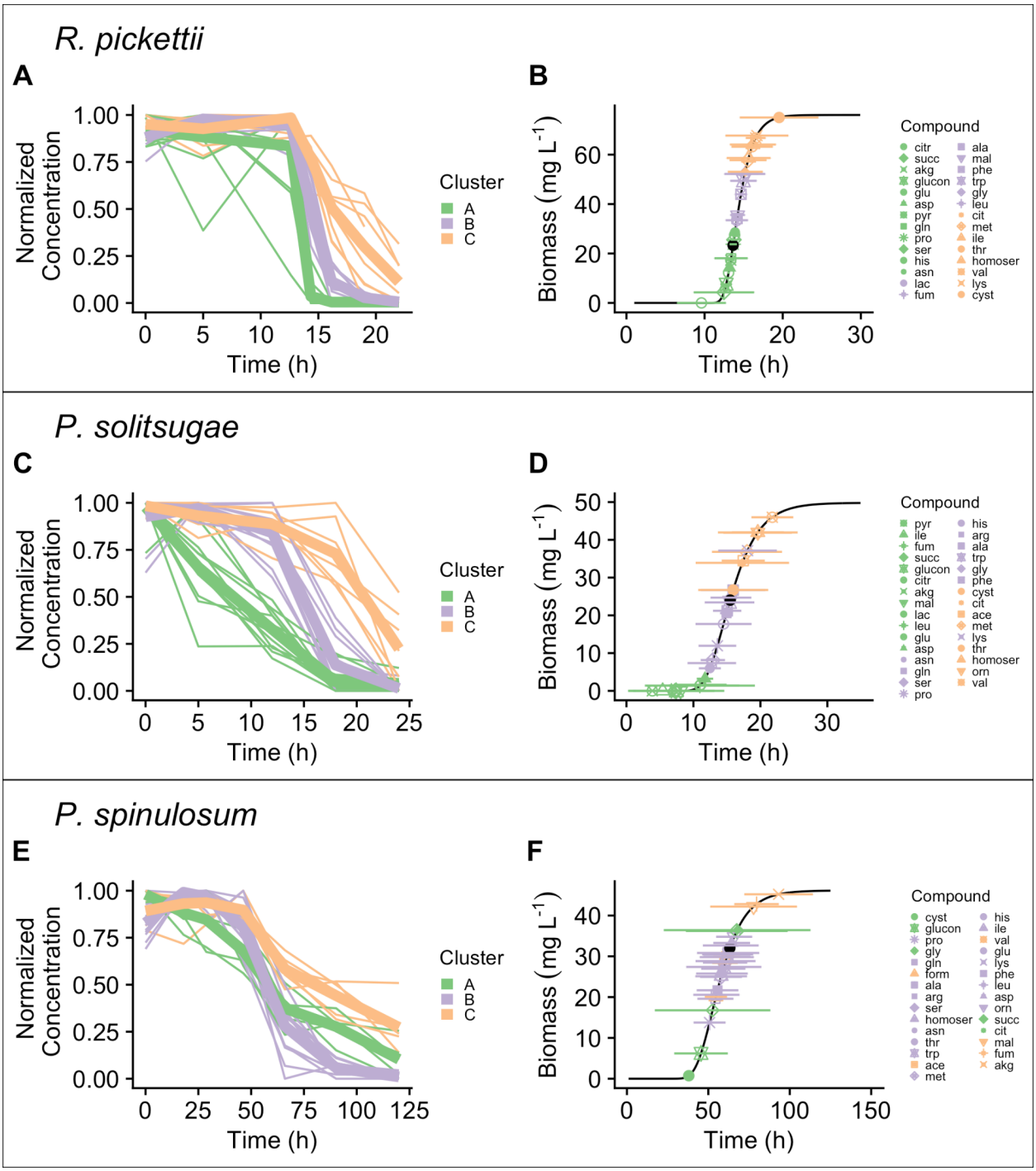

FIG 1 Depletion dynamics for observed LMWOS. Plots are paired by microbial isolate depicting depletion dynamics (A, C, E) and usage window plots (B, D, F) for uptake clusters identified using a k-means approach. Lines (A, C, E) are individual substrate uptake patterns normalized to initial concentration (mean, n = 3) with the thickest line showing the mean of the cluster. All

points in usage window plots (B, D, F) are the mean modeled midpoints of depletion (t_{50}) plotted over the growth curve of the isolate (black line). The mean midpoint of overall carbon depletion is shown with a black circle. Horizontal bars around each t_{50} show the usage window (10% - 90% of initial concentration). All substrates are colored by cluster and listed in the legend in order of increasing t_{50}. Ala, alanine; arg, arginine; asn, asparagine; cit, citrulline; cys, cysteine; glu, glutamate; gln, glutamine; gly, glycine; his, histidine; lys, lysine; met, methionine; orn, ornithine; ile, isoleucine; leu, leucine; lys, lysine; phe, phenylalanine; pro, proline; ser, serine; thr, threonine; trp, tryptophan; val, valine; ace, acetate; akg, α-ketoglutarate; form, formate; glucon, gluconate; lac, lactate; mal, malate; oxa, oxalate; pyr, pyruvate; succ, succinate.

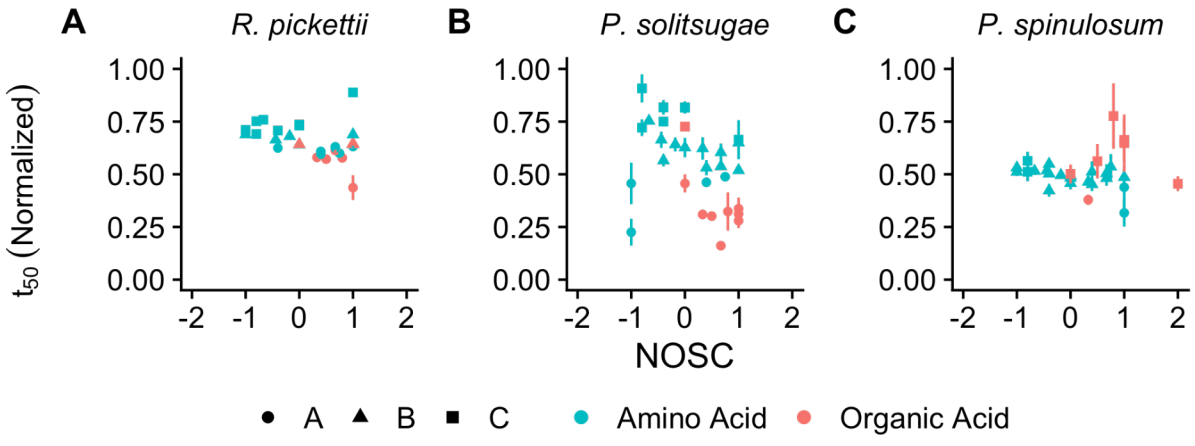

FIG 2 Inflection points of substrate depletion (t_{50}) normalized to stationary phase sampling time as a function of substrate oxidation state (NOSC). Normalized t_{50} values are the mean of three biological replicates with error bars representing standard error. Plots are paneled according to microbial isolate (A, B, C) and shapes illustrate cluster affiliation as determined using k-means clustering. Colors represent compound class (amino acid or organic acid).

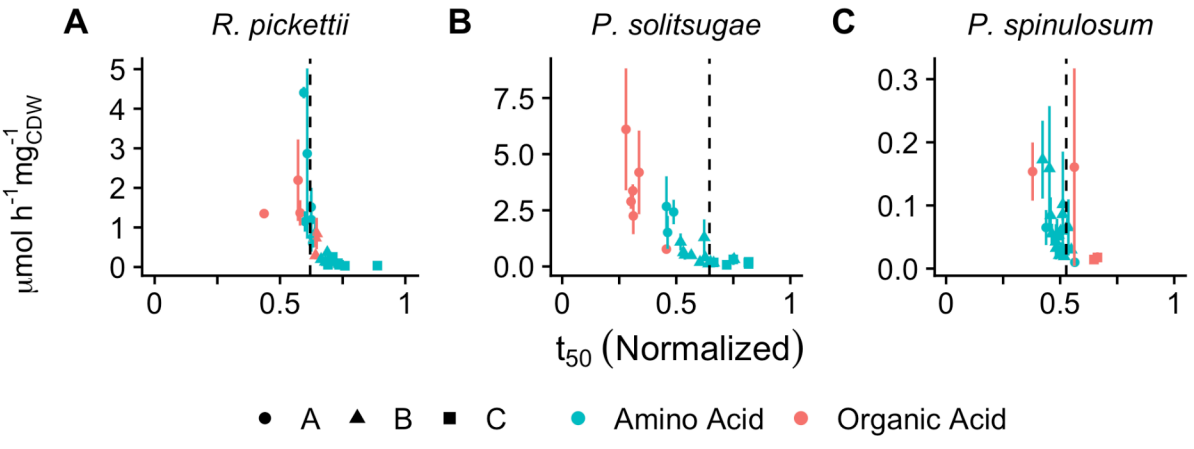

FIG 3 Biomass-normalized maximum depletion rate (A-C) as a function of the inflection point of depletion (t_{50}) normalized to stationary phase sampling time. Values are the mean of three biological replicates with error bars representing standard error. Shapes illustrate cluster affiliation and colors represent compound class (amino acid or organic acid). The vertical dashed line depicts the normalized t_{50} of overall carbon depletion from the media. Several points were removed for visualization purposes due to high variance between biological replicates (*P. solitsugae* – isoleucine, *P. spinulosum* – cystine & succinate).

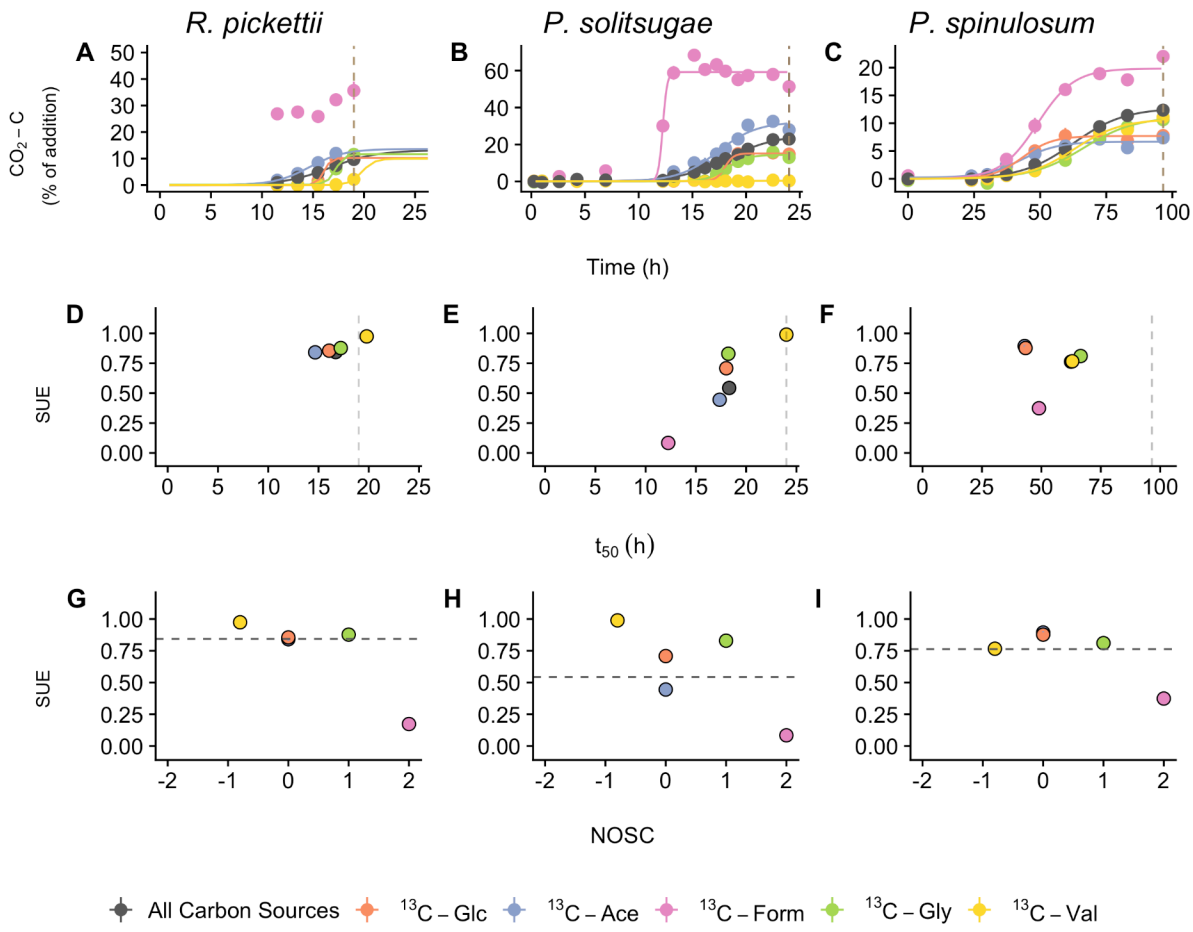

65

66 **FIG 4** Respiration dynamics of ^{13}C-labeled substrates and cumulative respiration along with
67 estimates of substrate use efficiency (SUE). Graphs are grouped vertically for the three microbial
68 isolates and arranged in order of decreasing specific growth rate (*R. pickettii* > *P. solitsugae* > *P.*
69 *spinulosum*). Panels display respiration as a function of time in the first row of panels (A-C),
70 SUE as a function of the midpoint of respiration, t_{50}, (D-F), and SUE as a function of substrate
71 oxidation state (G-I). The dashed vertical line in plots A-F indicates stationary phase of the
72 overall growth curve and the sample point for determination of ^{13}C present in microbial biomass.
73 The dashed horizontal line in plots G-I indicates the cumulative carbon use efficiency of all
74 carbon sources. See Fig. S6 for full panel A and Table S6 for microbial biomass carbon and
75 nitrogen composition data. Glc, glucose; Ace, acetate; Form, formate; Gly, glycine; Val, valine.

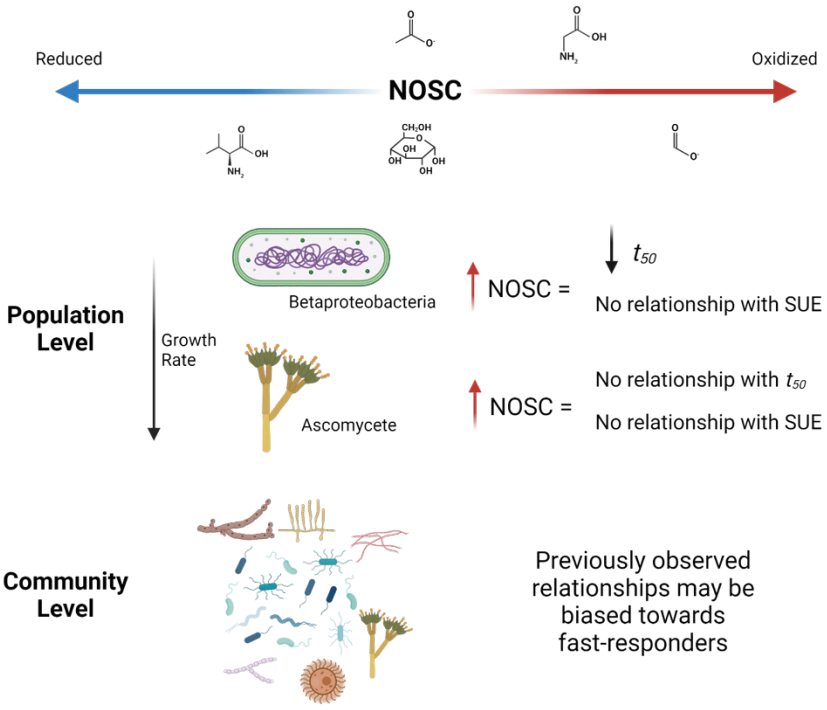

FIG 5 Summary chart outlining the results of this study and the possible implications at the community level. Created with BioRender.com.